

**FLODESIGN, INC.  
WILBRAHAM, MA. 01095**

REPORT No. FD 200801

**A New Analytical Model for  
Wind Turbine Wakes**

*by  
Michael, J. Werle, PhD*

**June 1, 2008**



# A New Analytical Model for Wind Turbine Wakes

*M. J. Werle, PhD<sup>1</sup>*

FloDesign Inc. Wilbraham, MA 01095

A new, closed form, analytical model is put forward for estimating the impact of a wind turbine on its immediate downstream neighbor as occurs in virtually all existing wind farms. It is first-principles based and overcomes past formulation limitations. The model, verified through comparison with a large compendium of measured results, provides a new pathway for addressing the critical issue of wind farm productivity prediction and design layout. It contains three critical elements: 1.) an exact model of the essentially inviscid near wake flow region 2.) a methodology for estimating the length of the intermediate wake based on Prandtl's turbulent shear layer mixing solution; and 3.) a far wake model based on the classical Prandtl/Swain axisymmetric wake analysis. The model's predictions reinforce results of recent studies of horizontal axis wind turbine farms indicating that longitudinal turbine spacing of less than 10 diameters lead to severe wake-induced productivity losses. The current model clearly shows that the fundamental root cause of this loss is the deep velocity deficit trough aft of the lead turbine that is only slowly overcome. The model also provides the basis for extending its application to downstream rows of turbines imbedded in a wind farm.

## Nomenclature

A	Flow cross sectional area
c	Circulation related constant of Eq. (1)
$C_p$	Power coefficient, see Eq. (3a)
$C_T$	Thrust coefficient, see Eq. (3b)
K	Absolute mixing-length related constant for the far wake region
$K_m$	Relative mixing-length related constant for the intermediate wake region
L	Nondimensional longitudinal distance between wind turbines, see Fig. 1
p	Pressure
P	Power
T	Thrust
u	nondimensional $V/V_a$
V	Velocity
W	Nondimensional lateral spacing between wind farm rows, see Fig. 1
x	Distance down-wind of a wind turbine
X	Nondimensional axial distance from a wind turbine, see Eq. (1)
$\rho$	fluid density

## Subscripts

a	ambient free stream conditions
d	conditions on down-wind side of wind turbine, see Fig. 3
i	inviscid or near wake region
o	downstream outlet conditions see Fig. 3
u	conditions on up-wind side of wind turbine, see Fig. 3
v	properties in the viscous or far wake
0	properties at far wake virtual origin
1,2,3	properties at wind turbines 1, 2 and 3 respectively in Fig. 1

---

<sup>1</sup> Chief Scientist, 380 Main Street, Wilbraham, MA 01095, AIAA Fellow

## **1. Introduction**

A large majority of the horizontal axis wind turbines (HAWTs) in use today are employed in wind farm arrays, such as that depicted schematically in Fig. 1. It has long been known that turbines' individual longitudinal and lateral displacements can strongly influence the wind farm's power generating efficiency. Placing the turbines too close together reduces the output of all downwind turbines due to the wake velocity deficits of upwind turbines while placing them too far apart reduces the number of turbines and thus the amount of energy extractable from a given property size. Both of these effects have direct negative influence on the cost of the power delivered. Recent studies (see Refs. 1-6 for example) show that even with the relatively large longitudinal and lateral separation distances of seven HAWT diameters, Turbines 2, 3 and beyond of Fig. 1 will sometimes deliver about 65% of the Turbine 1 power level. Therefore it is critically important to determine the optimal array configuration in order to maximize a wind farm's productivity.

Numerous attempts have been made to provide an accurate model for the velocities in wind turbine wakes (see Refs. 1-22) with a comprehensive review of the state-of-the-art as of 2003 provided by in Ref. 11 by Vemeer, Sorensen and Crespo. The fluid dynamic situation is complex not only analytically due to the merging of multiple wakes as one proceeds down a row of turbines (see Fig. 1) but it is also difficult to obtain definitive, reliable data for such large structures in open wind settings. The recent work of European teams and individual researchers (see Refs. 1-6) must be noted in this regard as it has begun to provide needed insights relative to the flow structure attendant to wind turbines in wind farms. It has also highlighted the fact that a successful basis for establishing a reliable analytical model for this has not yet emerged. In particular, there still exists uncertainty as to how to model the velocity deficit produced in the wake of an individual wind turbine (e.g., Turbine 1 of Fig. 1) as it mixes out with distance and therefore sets up the velocity field approaching a down-wind turbine such as Turbine 2 of Fig. 1.

The current effort focuses entirely on the first-turbine wake problem, i.e., modeling the influence of Turbine 1 on Turbine 2. It assumes large enough lateral spacing,  $W$ , such that Rows 2 and 3 induce negligible effects on Turbines 1 & 2 of Row 1. This is the core building block for wind farm modeling, which, to date, has not been satisfactorily attained. In the following sections, a first principals based Encouraging comparisons of the wake centerline velocities, second-turbine power degradation and wake growth rate are shown for a very wide collection of data including full scale wind turbines in both off shore or on-shore placements, as well as small scale wind turbine rotors and porous plate simulators tested in wind tunnels.

## **2. The Flow Structure in a Wind Turbine Wake**

As discussed in most reference texts and numerous papers (see Refs. 1-22), it is well documented and understood that a wind turbine wake, like all axisymmetric bodies, has three distinct regimes as depicted in Fig. 2; the near wake, the intermediate wake and the far wake. Each will be discussed briefly below in order to set the stage for the analytical models developed in the three sections that follow.

**The Near Wake:** The principle features of the near wake region of Fig. 2 relevant to current purposes are:

- The pressure rises ahead of the turbine as the capture streamtube expands to the blade's diameter, then drops abruptly across the turbine and thereafter increases steady in the near wake region to the free-stream value,  $p_a$ .
- The velocity inside the capture streamtube decreases as it approaches the turbine, remains constant across the turbine and thereafter decreases further in the near wake as the pressure rises downstream to  $p_a$ .
- The width of the near wake aft of the turbine (i.e., the capture streamtube) grows to a fixed diameter as the pressure approaches  $p_a$  and the velocity decreases to satisfy mass and momentum conservation.
- This region is dominated by inviscid processes and is known to be of the order of one prop diameter,  $D_p$ , in axial length.

**The Intermediate Wake:** The principle features of the intermediate wake region are:

- The pressure is constant and equal to  $p_a$ .

- The centerline velocity remains constant as turbulent mixing increase at the wake outer boundary due to the large radial gradient in the axial velocity.
- The initial lateral spread rate of the mixing layer can be approximated using Prandtl’s self-similar solution (Ref. 23 or see Refs. 24 & 25 for example) for the turbulent mixing of a planar velocity discontinuity.
- The length of this region is reported to be several diameters long and ends when the mixing layer reaches the centerline and initiates a change in the centerline velocity.

**The Far Wake:** The principle features of the far wake region are:

- The pressure remains constant and equal to  $p_a$ .
- The centerline velocity now begins a steady increase toward the free stream value,  $V_a$ , due to turbulent mixing. Prandtl and Swain (Refs. 24 & 27) provided first and second order accurate closed form, power-law solutions for this region using self-similarity concepts that scale with the momentum deficit induced by the wind turbine.
- The lateral spread rate of the mixing region was predicted by Prandtl and Swain to be governed by fractional powers of axial distance and the thrust coefficient of the wind turbine.
- The Prandtl/Swain solution contains two empirical constants: an “absolute” constant applicable to all axisymmetric wakes which must be determined from experiments, plus an arbitrary constant representing the virtual origin of the far wake which must be determined from the near and intermediate wake behavior.

To date, most published attempts to analytically model wind turbine wakes (see Refs. 1-6 for example) have not employed the details of the three phase structure of Fig. 2, but have focused principally on a far wake like structure. However, even within the far wake region, current models have not employed the thrust coefficient scaling (momentum deficit) dictated by the Prandtl/Swain exact solutions. The resulting models have generally shown either limited or unsatisfactory agreement with measured data. As a result many have turned to a single, empirically based, power-law scaling for the entire wake in an attempt to improve agreement with measured data. However, to date, none have led to satisfactory results.

In the following sections, these limitations will be relieved and it will be shown that: 1.) the near wake centerline velocity decay can be calculated from a well documented, simple, exact closed form solution of the vorticity equations that was originally developed for propeller-based propulsion; 2.) the Prandtl/Swain far wake analytical model’s applicability is verified through comparisons with a very large compendium of wind turbine related measurements; and 3.) an algebraically simple composite solution for the entire wake can be constructed using Prandtl’s self-similar solution for a lateral velocity discontinuity to couple the near and far wake solutions. Very encouraging comparisons are provided with measured centerline velocity decay, second turbine power degradation and lateral wake growth rate for a wide range of thrust coefficients. The implications of the model’s prediction for wind farm spacing and productivity levels are also discussed.

### **3. The Near Wake Region**

As depicted in Fig. 3 for a typical HAWT, the near wake will be considered to be governed by inviscid pressure forces with the turbulent mixing layer that initiates at the turbine having negligible effect to first order on the flow structure. McCormick (Ref. 27, pp 96-98) provides the exact solution of the Biot Savart Law applied to the spiraling vorticity field aft of a lifting prop to write the nondimensional inviscid centerline velocity,  $u_i$ , anywhere within the capture streamtube as:

$$u_i = 1 + c \left[ 1 + \frac{2X}{\sqrt{1 + 4X^2}} \right], \quad (1a)$$

where  $c$  is related to the total circulation induced by the wind turbine and

$$X \equiv x/D_p \quad . \quad (1b)$$

For current purposes,  $c$  can be determined by matching the predicted outlet velocity at downstream infinity,  $u_o$  of Fig. 3, to that predicted through use of a momentum balance and actuator disk theory (see Refs.20-22, or 28 for example) to write that

$$u_i = 1 - \frac{1 - u_o}{2} \left[ 1 + \frac{2X}{\sqrt{1 + 4X^2}} \right]. \quad (2a)$$

With this, the width,  $D_i$  of the capture streamtube can be calculated from mass conservations as:

$$D_i/D_p = \sqrt{\frac{1 + u_o}{2u_i}}. \quad (2b)$$

From any of Refs. 20-22 or 28, the outlet velocity,  $u_o$ , can be determined from either of the following relations:

Power Coefficient: 
$$C_P \equiv \frac{P}{\frac{1}{2} \rho A_p V_a^3} = \frac{u_p A_p (p_u - p_d)}{\frac{1}{2} \rho A_p V_a^3} = \frac{1}{2} (1 + u_o) (1 - u_o^2). \quad (3a)$$

Thrust Coefficient: 
$$C_T \equiv \frac{T}{\frac{1}{2} \rho A_p V_a^2} = \frac{A_p (p_u - p_d)}{\frac{1}{2} \rho A_p V_a^2} = (1 - u_o^2). \quad (3b)$$

As indicated in Section 2 above, the far wake scales with the Thrust Coefficient,  $C_T$ , which will be taken here as the controlling parameter for the entire problem. Thus Eqs. (3a)-(3b) can be inverted to write that:

$$u_o = \sqrt{1 - C_T}, \quad (4a)$$

and

$$C_P = \frac{1}{2} C_T [1 + \sqrt{1 - C_T}]. \quad (4b)$$

Figures 4(a) and 4(b) provide the resulting values of the centerline velocity,  $u_i$ , and wake growth rate,  $D_i/D_p$  for a complete range of  $C_T$  up to the stall limit,  $C_T=1$ . The case of  $C_T = 8/9$  corresponds to attainment of the maximum power output, i.e., the Betz Limit of  $C_p=16/27$ . Two important observations can be made here that will be of value in what follows:

1. Upstream of the HAWT, the centerline velocity and capture streamtube very clearly attain their asymptotic levels within one to two diameters regardless of the thrust level, especially for  $C_T < 8/9$ .
2. Downstream of the HAWT, both the centerline velocity and capture streamtube take longer to attain their asymptotic levels. For  $C_T < 8/9$  (Max Power level) they effectively reach their limit values at  $X=2$  while for  $C_T > 8/9$ ,  $X$  increase to four or more as stall is approached.

The centerline velocity results of Fig. 4(a) can be used to begin to assess the influence of the turbine longitudinal spacing of Fig. 1 on the power degradation from Turbine 1 to 2. Using the definition given in Eq. (3a), one can write the power ratio as:

$$\frac{P_2}{P_1} = \left( \frac{V_2}{V_a} \right)^3 \frac{C_{T2} \left[ 1 + \sqrt{1 - C_{T2}} \right]}{C_{T1} \left[ 1 + \sqrt{1 - C_{T1}} \right]} \quad (5)$$

where  $V_a$  is the upstream ambient wind speed approaching Turbine 1 and  $V_2$  is the effective wind speed approaching Turbine 2. The ratio  $V_2/V_a$  of Eq. (5) is merely Turbine 1's wake velocity,  $u_i$ , calculated by evaluating Eq. (2a) at a value of  $X < L$  to account for the upstream propagation effect discussed in item 1 directly above. Thus, for current purposes:

$$V_2/V_a = u_{i2} = 1 + \frac{1 - u_0}{2} \left[ 1 + \frac{2(L-1)}{\sqrt{1 + 4(L-1)^2}} \right] \quad (6)$$

The Turbine 1 Thrust Coefficient,  $C_{T1}$  of Eq. (5), is known but the corresponding value for Turbine 2,  $C_{T2}$ , must, in general, be determined from the performance characteristics of the particular HAWT being employed. For the purpose of demonstrating the current model in a generic fashion, it will be assumed here the HAWT employed has a somewhat idealized thrust and power curves as depicted in Fig. 5, i.e. a relatively flat thrust curve up to the turbines rated power level. With this, as shown in Fig 5, it is reasonable to assume that the thrust coefficients are approximately equal in Eq. (5). Relief of this constraint can be applied straightforwardly for any particular HAWT application of interest.

Figure 6 provides the resulting power ratios predicted using Eqs. (5) & (6) for the full range of Thrust Coefficients and longitudinal spacing up to  $L = 5$ . Not surprisingly, the levels become extremely low as the Max Power situation is approached and are seen to continue towards zero as the stall level is approached. Clearly these low levels would be unacceptable in any practical sense and indicate why it is necessary to call on the turbulent mixing in the intermediate and far wake regions to help increase the centerline velocity and improve the power production situation.

#### **4. The Far Wake Region**

It is useful to next give attention to modeling of the far wake region, which, in turn, will also establish the pathway by which the three regions become analytically linked for ultimate closure. To that end, Swain's work (Ref. 26), performed in collaboration with Prandtl, extended his earlier analysis (Ref. 23) to include higher order terms in the asymptotic analysis. For current purposes, use will be made of the first order approximation to write the viscous wake growth rate,  $D_v$ , as given by Swain as:

$$D_v/D_p = K(C_T X)^{1/3}, \quad (7a)$$

and the attendant viscous induced centerline velocity,  $u_v$ , as:

$$u_v = 1 - \frac{\left( C_T^{1/2}/X \right)^{2/3}}{2K^2}. \quad (7b)$$

Here, the constant  $K$  is related to Prandtl's turbulent mixing length and was designated by Swain as a "universal" constant, i.e. one that must be determined from experiments and will be the same for all axisymmetric bodies generating a momentum deficit in a uniform stream, so long as the turbulent mixing length hypothesis is valid.

In the current study, K has been determined from a compendium of over 104 data points collected from Refs. 1-10 (and their reference works) covering model wind turbine rotors tested in wind tunnels, full size wind turbines located in wind farms both on and off shore, and porous disc wind turbine simulators tested in a wind tunnel. All the results are provided in Table 1 and Appendices A-D discuss each data set in detail. These are all provided in Figs. 7(a) & (b) indicating a wide range of velocity defects and wake growth rates for values of X from 1 to 15, and as indicated in Table 1, for Thrust Coefficient levels from 0.26 to 0.92. Figures 7 (c) & (d) provide the same results in terms of the scaled variables indicated by Eqs. (7a) & 7(b). These later results are further employed to evaluate K from Eqs. (7a) & (7b) as:

$$K = \frac{D_v/D_p}{\left(C_T X\right)^{1/3}} = \frac{\left(C_T^{1/2}/X\right)^{1/3}}{\left(2[1-u_v]\right)^{1/2}} \quad (8)$$

The results shown in Figures 7(e) & 7(f) indicate a clear convergence of K to unity from below and above respectively as the scaled axial distances increase.

With this in hand, following Swain's suggestion, one can then write the more general form of the asymptotic far wake model by introducing the virtual origin,  $X_0$ , so that:

$$u_v = 1 - \frac{1}{2} \left[ \frac{C_T^{1/2}}{X - X_0} \right]^{2/3} \quad (9a)$$

$$D_v/D_p = \left[ C_T (X - X_0) \right]^{1/3} \quad (9b)$$

The value of  $X_0$ , the location of the virtual origin of the wind turbine's far wake region, must be determined through coupling of the far, intermediate and near wake relations as discussed in Sections 5 & 6 below.

### **5. The Intermediate Region**

There is no self similar solution available for this region due to its axisymmetric nature and finite diameter. However, one can employ Prandtl's solution for turbulent mixing at a planar velocity discontinuity (see Ref, 24 for example) to establish an estimate to the length of the intermediate wake region. This in turn will be used to establish  $X_0$  and ultimately couple all three regions together. Referring to Fig. 8, the intermediate wake region begins at a point near  $X_i$  and ends at  $X_m$ , when the shear layer penetrates to the centerline. Near  $X_i$ , the shear layer thickness is small compared to the radial distance,  $R_i = D_i/2 = D_0/2$ , and Prandtl's results apply, predicting a linear growth rate for the shear layer width. Using this as a means of estimating  $X_m$ , one arrives at the relation:

$$X_m = X_i + K_m \frac{D_o}{D_p} \frac{1+u_o}{1-u_o} \quad (10)$$

where the value of  $K_m$  has to be established from experimental data. Also, from the discussion of Section 3 above,  $X_i$  is here taken to be 2 and the diameter of the near wake at  $X_i$  is given by Eq. (2b).

## 6. The Composite Wake Model

Figure 9 depicts the method employed to complete the analysis. The far wake model is coupled to the near wake by setting the virtual origin of the far wake,  $X_0$ , such that the two velocities,  $u_i$  and  $u_v$ , are equal at the match point,  $X_m$ , determined from Eq. (10). The resulting wake centerline velocity relations are:

$$\text{For } X < X_m, \text{ Eq. (2a) gives } u_w = 1 + \frac{1 - u_0}{2} \left[ 1 + \frac{2X}{\sqrt{1 + 4X^2}} \right]. \quad (11a)$$

$$\text{For } X > X_m, \text{ Eq. (9a) gives } u_w = 1 - \frac{1 - u_m}{\left[ (X - X_m) \left( 2[1 - u_m] \right)^{3/2} / C_T^{1/2} + 1 \right]^{2/3}}, \quad (11b)$$

where

$$u_m = 1 + \frac{1 - u_0}{2} \left[ 1 + \frac{2X_m}{\sqrt{1 + 4X_m^2}} \right], \quad (11c)$$

and  $X_m$  is given by Eq. (10).

Similarly, the resulting wake growth rate relations are:

$$\text{For } X < X_m, \text{ Eq. (2b) gives } D_w / D_p = \sqrt{\frac{1 + u_0}{2u_w}}. \quad (12a)$$

$$\text{For } X > X_m, \text{ Eq. (9b) gives } D_w / D_p = D_m / D_p \left[ C_T (X - X_m) / \left( (D_m / D_p)^3 + 1 \right) \right]^{1/3}, \quad (12b)$$

where

$$D_m / D_p = \sqrt{\frac{1 + u_0}{2u_m}}. \quad (12c)$$

Note the solution remains dependent on the constant,  $K_m$  of Eq. (10) which is related inversely to the turbulent mixing length for the intermediate wake region.

As an example calculation, Figure 10(a) shows the two components of the centerline velocity solution plus the composite solution for  $K_m=0.1$  at the maximum power case,  $C_T=8/9$ . The most significant aspect of the velocity profiles shown in Fig. 10(a) is the relatively contorted variation in the velocity as it starts with a low value at the turbine, then decreases further quite rapidly in the near wake after where it reverses itself and begins an initially rapid but ultimately rather surprisingly slow growth toward the free stream value. As shown in Fig. 10(b) as the constant,  $K_m$ , increases (decreasing mixing length), the match point moves downstream as expected. The case of

$K_m = 0$  corresponds to an infinitely large mixing length and thus an intermediate wake region length of zero. Similarly, an infinitely large  $K_m$  corresponds to a mixing length of zero and would thus produce an infinitely long intermediate wake length.

To obtain an estimate to the applicable value of  $K_m$  for wind turbines, the data sets shown in Fig. 7 were again employed. In this regard, it is first worthy of note that, aside from the value of  $K_m$ , the composite model of Eqs. (11) & (12) contains only one parameter,  $C_T$ , that characterizes the wind turbine's influence on the flow structure. Thus the data sets of Table 1 and Appendices A-D, were first grouped into eight  $C_T$  levels about which  $C_T$  varied by less than 5%. These are given in Table 2. Solutions were generated for the velocities and wake growth rates using Eqs. (11) and (12) and the power degradation ratios using Eq. (5) for each  $C_T$  level.  $K_m$  was then varied to achieve a visually good fit, which in this case was found to be with  $K_m = 0.1$ . The resulting comparisons are provided in Figs. 11 and 12 for  $C_T$  ranging from 0.26 to 0.92. Overall, the analytical results show consistently good qualitative agreement with the data trends and remarkable agreement quantitatively for all conditions, especially when one considers the wide range of measurement conditions and techniques employed. It is most satisfying to see that all the data sets do appear to strongly reflect elements of the three tiered structure employed in the current analysis. In particular, it is seen that the presence of the near and intermediate wake is essential to setting up the proper approach to the far wake region. The analytical wake velocities shown in Fig. 11 consistently track the measured values and, as such, expose their embedded three trends, which would be difficult to decipher without the model's guidance. This is also especially relevant to the prediction and data comparisons of the power degradation ratio,  $P_2/P_1$ , as shown in Figs. 11 (b), (c), (e) and (f) where the low values in the near wake region near  $L = 2$  are well represented and seen to set the basis for the relatively low values measured at  $L = 7$  and 9

The wake growth results shown in Fig. 12 again highlight the three embedded trends: a rapidly expanding near wake, an intermediate wake whose length shrinks as  $C_T$  increases and a far wake growth rate that increases as  $C_T$  increases. Most interestingly, these results indicate two additional trends: the wake width is very sensitive to  $C_T$  and even a distance of 16 diameters down-wind, the wake never exceeds 2.5 diameters in width.

Fig. 13 provides a summary of results of the current analysis for a range of thrust coefficient,  $C_T$ , from 0.2 to 0.99, the latter being very near stall. Seen in this form, most notable is the very large variation in the wake structure for the typical range over which one expects a HAWT to operate. The flow structure and performance is clearly dominated by the sometimes large velocity trough in the near wake seen in Fig. 13(a). Even though the velocities asymptotically merge rather quickly in the far wake, they all suffer from an initial deficit and recover very slowly toward the free stream value. One has to be over six diameters downstream to see reasonable velocity recovery which does not begin to attain the 90% level until nine or more diameters distance.

In Fig. 13(b), the wake growth rates show a much higher sensitivity to the thrust level and are worrisome because of their implications for possible interference with the ground plane for a typical HAWT tower height of 1 to 1.5 turbine diameters. Here, the variation in the intermediate wake is seen to be one of the controlling elements of the far wake growth. These wake growth predictions do not indicate row to row interference for Turbines 2 for up to 10 diameters and well beyond for a typical HAWT lateral spacing of  $W = 5$  or more.

Finally, the power degradation ratios,  $P_2/P_1$ , shown in Fig. 13 (c) are also very worrisome because of the low values of 0.6 to 0.7 produced for nearly all but the lowest thrust levels, even up to  $L=10$ . It should be borne in mind that these predictions can only be viewed as a guide and that the model must be adapted to the particular HAWT performance characteristics, i.e., the dependency of the thrust coefficient on the wind speed in Eq. (5), in order to obtain accurate predictions for a particular configuration and wind environment.

## **7. Summary and Conclusions**

A first-principles based, closed form analytical model is now available for estimating the impact of a wind turbine on its immediate down-wind neighbor. The model employs two "universal constants" related to Prandtl's turbulent mixing length. Its verification, established herein through comparison with a new and large compendium of measured results, provides a new direction and pathway for addressing the critical issue of wind farm design layout and productivity. The model contains three critical elements that should be accounted for and accommodated in all future wind turbine wake analyses efforts:

1. A model of the essentially inviscid near wake flow regime that is critical to setting the initial conditions for the development of the downstream flow structure.
2. A methodology for estimating the length of the intermediate wake and thus the effective starting point of the far wake.
3. A far wake model based on the Prandtl/Swain analysis and scaling.

The model verifies and reinforces what has begun to become apparent in recent studies of HAWT wind farms. For longitudinal spacing of less than 10 diameters, they can suffer significant wake induced productivity losses. The fundamental root cause of this is the deep velocity trough encountered aft of the lead turbine, the impact of which persists into the far wake. Because this is a result of the basic aerodynamics of HAWTs, it cannot be controlled or overcome. As such, it should be accounted for in all future cost analyses of wind farm output potential using the specific performance characteristics of the HAWT employed to tune the model accordingly.

With this model in hand, attention can now be turned to its generalization for third and beyond rows in a wind farm. One approach that should be considered would be to combine the effects of the Rows' 1 & 2 thrust deficits into a single element influencing the Prandtl/Swain far wake development approaching the third row and so on. The model elements for the near and intermediate wakes of Turbine 2 would be essentially the same as that of Turbine 1 adjusted accordingly. It is also apparent that there is a need for more and more precise measurements of wind turbine wake centerline velocities for further verification and refinement of the model.

## References

1. Barthelmie, R.J., Frandsen, S.T., Rethore, P.E., Mechali, M., Pryor, S.C., Jensen, L., and Sorensen, P., "Modeling and measurements of offshore wakes", presented at OWEMES Conf, Citavecchia, Italy, April 22-23, 2006
2. Rathmann, O., Barthelmie, R.J. and Frandsen, S., "Turbine wake Model for Wind Resource Software", presented at EWEC Wind Energy Conference Conf, 2006
3. Rathmann, O., Frandsen, S. and Barthelmie, R., "Wake Modeling for intermediate and large wind farms", paper BL199 presented at EWEC Wind Energy Conference Conf, 2007
4. Barthelmie, R.J., Rathmann, O., Frandsen, S.T., Hansen, K., Politis, E., Prospathopoulos, J., Rados, K., Cabezon, D., Schlez, W., Phillips, J., Neubert, A., Schepers, J.G. and van der Pijl, S.P., "Modeling and measurements of wakes in large wind farms", Journal of Physics Conference Series, **The Science of Making Torque from Wind**, Vol. 75, 2007.
5. Mechali, M., Jensen, L., Barthelmie, R., Frandsen, S., and Rethore, P.E., "Wake effects at Horns Rev and their influence on energy production", presented at European Wind Energy Conference, Athens Greece, October 2006
6. Barthelmie, R.J., Folkerts, L., Ormel, F.T., Sanderhoff, P., Eechen, P.J., Stobbe, O. and Nielsen, N.M., "Offshore Wind Turbine Wakes Measured by Sodar", Journal of Atmospheric and Oceanic Technology, Vol. 20, pp 466-477, 2003.
7. El Kasmi, A. and Masson, C., "An extended  $k-\epsilon$  model for turbulent flow through horizontal-axis wind turbines" Journal of Wind Engineering and Industrial Aerodynamics, Vol. 96, pp 103-102, 2008.
8. Magnusson, M., "G., Near-wake behavior of wind turbines", Journal of Wind Engineering and Industrial Aerodynamics, Vol. 80, pp 147-167, 1999.
9. Ainslie, J.F., "Calculating the Flowfield in the wake of wind turbines", Journal of Wind Engineering and Industrial Aerodynamics, Vol. 27, pp 213-224, 1988.
10. Sforza, P.M., Sheerin, P. and Smoroto, M., "Three-Dimensional Wakes of Simulated Wind Turbines", AIAA Journal, Vol. 19, No. 9, pp 1101-1107, September 1981.
11. Vermeer, L.J., Sorensen, J.N., and Crespo, A., "Wind turbine wake aerodynamics", published in **Progress in Aerospace Sciences**, Vol. 39, pp. 467-510, 2006.
12. Lissman, P.B.S., "Energy Effectiveness of Arbitrary Arrays of Wind Turbines", Journal of Energy, Vol. 3, No. 6, pp 323-327, Nov.-Dec. 1979
13. Lissman, P.B.S., Zalay, A. and Gyatt, G.W., "Critical Issues in the Design and Assessment of Wind Turbine Arrays", Presented at the International Symposium on Wind Energy Systems, Stockholm, Sweden, December 21-24, 1982.

14. Katic, I., Hojstrup, J., and Jensen, N.O., "A Simple Model for Cluster Efficiency", Presented at European Wind Energy Conference, Rome, Italy, October 7-9, 1986.
15. Albers, A., Beyer, H.G., Kramkowski, T., Schield, M., Schomburg, A., Schlez, W., Waldl, H. And de Witt, U., „Results from a joint wake interference research program“, presented at the European Community Wind Energy Conference, Ioback-Travemunde, Germany, March 8-12, 1993
16. Rados, K., Larsen, G., Barthelmie, R.J., Schlez, W., Lange, B., Schepers, G., Hegberg, T. and Magnisson, M., "Comparisons of Wake Models with data for Offshore Windfarms", *Wind Engineering*, Vol. 25, No. 9 pp 271-280, 2001.
17. Seifert, H. and Kronig, J., "Recommendations for Spacing in Wind Farms", Presented at the European Wind Energy Conference, Madrid, Spain, June 17, 2003.
18. Norgaard, P. and Holttinen, H., "A Multi-turbine Power Curve Approach", Presented at the Nordic Wind Power Conference, Chalmers University of Technology, Gothenberg, Sweden, March 1-2, 2004.
19. Frandsen, S., Barthelmie, R., Pryor, S., Ratmann, O., Larsen, S., Hojstrup, J. and Thorgersen, M., "Analytical Modeling of Wind Speed Deficit in Large Offshore Wind Farms", *Wind Energy*, Vol. 9 pp 39-53, 2006.,
20. Gashe, R. and Twele, J.: **WIND POWER PLANTS**, Solarpraxis, 2002
21. Hau, Eric, **Wind Turbines**, Second Edition, Springer Publishing Company, 2005.
22. Manwell, J.F., McGowan, J.G., and Rogers, A.L., **WIND ENERGY EXPLAINED, Theory, Design and Application**, John Wiley & Sons, LTD, West Sussex England, 2002
23. Prandtl, L., "The mechanics of viscous flows", appearing in the Proceedings of the 2<sup>nd</sup> International Conference of Applied Mechanics, p 62, Zurich, Switzerland, 1926 and in **Aerodynamic Theory** p 166 by W. F. Durand, , 1935.
24. Schlichting, H., **Boundary Layer Theory, Fourth Edition**, McGraw Hill Book Company, 1960.
25. Tennekes, H. and Lumley, J.L., **A First Course in Turbulence**, MIT Press, 1972
26. Swain, L.M., "On the Turbulent Wake Behind a Body of Revolution" Proceedings of the Royal Society of London. Series A, Vol. 125, No.799, pp 647-659, November 1, 1929.
27. McCormick, Barnes W. Jr., **AERODYNAMICS OF V/STOL FLIGHT**, Dover Publications, Minneola NY, 1999
28. Werle, M.J., and Presz, Jr., W.M., "Ducted Wind/Water Turbines and Propellers Revisited", *Technical Note accepted for publication in the AIAA Journal of Propulsion and Power*, June 2007

**Table 1: Wake Database (yellow highlight implies calculated from Ref'd. data)**

	WS Range	Avg Wind Speed (m/s)	P <sub>1</sub> (MW)	P <sub>2</sub> /P <sub>1</sub>	P <sub>2</sub>	V <sub>2</sub> /V <sub>a</sub>	V <sub>2</sub>	C <sub>p</sub>	C <sub>T</sub>	L	x/Dp	D <sub>w</sub> /D <sub>p</sub>	Ref
Off Shore Horn Rev	8.5-9.5	9	0.946	0.730	0.691	0.890	8.010	0.422	0.667	9.4	8.4	1.845	2 Rathmann et al
(Vestas 80)	11.5-12.5	12	1.809	0.717	1.297	0.840	10.080	0.340	0.451	7	6	1.295	2 Rathmann et al
	8.5-9.5	9	0.946	0.607	0.575	0.840	7.560	0.422	0.667	7	6	1.575	2 Rathmann et al
	8.0-9.0	8.5	0.817	0.618	0.5054	0.853	7.250	0.432	0.695	7	6	1.664	3 Rathmann et al
	11.5-12.5	12	1.809	0.775	1.4012	0.876	10.510	0.340	0.340	7	6	1.250	3 Rathmann et al
	8.0-9.0	8.5	0.817	0.634	0.5183	0.860	7.310	0.432	0.695	7	6	1.699	3 Rathmann et al
	11.5-12.5	12	1.809	0.876	1.5848	0.923	11.070	0.340	0.451	7	6	1.775	3 Rathmann et al
	8.0-9.0	8.5	0.817	0.804	0.6572	0.927	7.880	0.432	0.695	9.4	8.4	2.267	3 Rathmann et al
	11.5-12.5	12	1.809	0.876	1.5848	0.923	11.070	0.340	0.451	9.4	8.4	1.775	3 Rathmann et al
	8.0-9.0	8.5	0.817	0.735	0.6004	0.901	7.660	0.432	0.695	9.4	8.4	1.975	3 Rathmann et al
	11.5-12.5	12	1.809	0.835	1.5105	0.903	10.840	0.340	0.451	9.4	8.4	1.606	3 Rathmann et al
	5.5-6.5	6	0.280	0.645	0.1803	0.870	5.222	0.420	0.662	7	6	1.712	4 Barthelmie et al
	7.5-8.5	8	0.688	0.585	0.4026	0.843	6.741	0.437	0.714	7	6	1.640	4 Barthelmie et al
	9.5-10.5	10	1.277	0.61	0.7792	0.835	8.353	0.415	0.615	7	6	1.495	4 Barthelmie et al
	7.5-8.5	8	0.688	0.7	0.4817	0.893	7.140	0.437	0.714	9.4	8.4	1.928	4 Barthelmie et al
	7.5-8.5	8	0.688	0.748	0.5148	0.912	7.294	0.437	0.714	10.5	9.5	2.105	4 Barthelmie et al
	8.0-10	9	0.946	0.624	0.5905	0.847	7.621	0.422	0.667	7	6	1.603	5 Mechali et al
	7.0-8.0	7.5	0.559	0.677	0.3785	0.882	6.614	0.430	0.714	7	6	1.851	5 Mechali et al
	8.0-9.0	8.5	0.817	0.71	0.5802	0.894	7.598	0.432	0.695	7	6	1.914	5 Mechali et al
	9.0-10	9.5	1.118	0.716	0.8007	0.888	8.436	0.424	0.643	7	6	1.798	5 Mechali et al
	7.0-8.0	7.5	0.559	0.709	0.3964	0.894	6.708	0.430	0.714	9.4	8.4	1.944	5 Mechali et al
	8.0-9.0	8.5	0.817	0.767	0.6268	0.913	7.762	0.432	0.695	9.4	8.4	2.094	5 Mechali et al
	9.0-10	9.5	1.118	0.663	0.7414	0.864	8.206	0.424	0.643	9.4	8.4	1.653	5 Mechali et al
	7.0-8.0	7.5	0.559	0.539	0.3014	0.819	6.141	0.430	0.714	7	6	1.551	5 Mechali et al
	8.0-9.0	8.5	0.817	0.505	0.4127	0.799	6.794	0.432	0.695	7	6	1.472	5 Mechali et al
	9.0-10	9.5	1.118	0.5	0.5591	0.789	7.500	0.424	0.643	7	6	1.391	5 Mechali et al
Off Shore MiddleGrunden		6	0.259	0.162	0.0419	0.708	4.248	0.523	0.662	2.4	1.4	1.265	2 Rathmann et al
(Bonus 76)		9	0.883	0.181	0.1602	0.570	5.130	0.526	0.667	2.4	1.4	1.166	2 Rathmann et al
		12	1.728	0.344	0.5936	0.657	7.884	0.392	0.451	2.4	1.4	1.000	2 Rathmann et al
Off Shore Vindeby	10.24-10.84	10.540				0.640		0.498	0.550		3.8	1.093	6 Barthelmie et al
	8.33-9.19	8.760				0.870		0.430	0.670		6.5	1.721	6 Barthelmie et al
	8.33-9.19	8.760				0.470		0.430	0.670		4.1	1.160	6 Barthelmie et al
	5.54-5.94	5.740				0.630		0.427	0.855		2.8	1.354	6 Barthelmie et al
	5.54-5.94	5.740				0.700		0.427	0.855		3.6	1.427	6 Barthelmie et al
	5.54-5.94	5.740				0.790		0.427	0.855		4.5	1.605	6 Barthelmie et al
	6.12-6.62	6.370				0.760		0.435	0.820		3.4	1.499	6 Barthelmie et al
	6.31-7.49	6.900				0.560		0.421	0.820		1.7	1.290	6 Barthelmie et al
	7.09-7.99	7.540				0.650		0.421	0.760		2.9	1.292	6 Barthelmie et al
	5.38-6.86	6.120				0.890		0.435	0.760		7.4	1.970	6 Barthelmie et al
	7.63-8.65	8.190				0.730		0.439	0.700		3.4	1.333	6 Barthelmie et al
	7.63-8.65	8.190				0.780		0.439	0.700		5	1.428	6 Barthelmie et al
Off Shore (Nibe B)		8.500				0.463			0.820		2.5	1.284	7 Kasmi et al
		8.500				0.722			0.820		6	1.429	7 Kasmi et al
		8.500				0.843			0.820		7.5	1.760	7 Kasmi et al
		9.560				0.516			0.770		2.5	1.242	7 Kasmi et al
		9.560				0.744			0.770		6	1.423	7 Kasmi et al
		9.560				0.882			0.770		7.5	1.926	7 Kasmi et al
		11.520				0.540			0.670		2.5	1.161	7 Kasmi et al
		11.520				0.701			0.670		6	1.265	7 Kasmi et al
		11.520				0.758			0.670		7.5	1.352	7 Kasmi et al
Off Shore (Danwin 180)		7.000	38.243			0.532			0.843		1	1.301	8 Magnusson
		8.000	63.784			0.379			0.820		1	1.320	7 Kasmi et al
		10.000	111.216			0.479			0.714		1	1.196	8 Magnusson
		8.000	63.784			0.438			0.820		4.15	1.291	7 Kasmi et al
		8.000	63.784			0.796			0.820		9.4	1.590	7 Kasmi et al
		11.000	137.973			0.641			0.650		6.2	1.189	7 Kasmi et al
Wind Tunnel Rotor Test						0.504			0.780		2.990	1.249	9 Ainslie
						0.657			0.780		5.043	1.316	9 Ainslie
						0.792			0.780		6.799	1.540	9 Ainslie
						0.901			0.780		10.167	2.093	9 Ainslie
Wind Tunnel Rotor Test						0.202			0.840		1.983	1.614	9 Ainslie's Ref 11
						0.603			0.840		4.098	1.324	9 Ainslie's Ref 11
						0.825			0.840		8.127	1.707	9 Ainslie's Ref 11
Wind Tunnel Rotor Test						0.625			0.540		1.983	1.073	9 Ainslie's Ref 10
						0.737			0.540		3.002	1.180	9 Ainslie's Ref 10
						0.796			0.540		4.098	1.289	9 Ainslie's Ref 10
						0.902			0.540		7.057	1.748	9 Ainslie's Ref 10
OnShore Wind Farm						0.659			0.700		2.971	1.248	9 Ainslie's Ref 13
						0.770			0.700		4.987	1.405	9 Ainslie's Ref 13
						0.903			0.700		6.987	2.001	9 Ainslie's Ref 13
OnShore Wind Farm						0.698			0.640		2.971	1.232	9 Ainslie's Ref 13
						0.834			0.640		4.987	1.519	9 Ainslie's Ref 13
						0.909			0.640		6.768	1.969	9 Ainslie's Ref 13
OnShore Wind Farm						0.707			0.600		3.979	1.204	9 Ainslie's Ref 12
OnShore Wind Farm						0.506			0.800		1.995	1.265	9 Ainslie's Ref 3
						0.776			0.800		3.926	1.516	9 Ainslie's Ref 3
						0.901			0.800		7.958	2.121	9 Ainslie's Ref 3
						0.930			0.800		9.686	2.487	9 Ainslie's Ref 3
						0.548			0.670		2.520	1.163	9 Ainslie's Ref 3
						0.744			0.670		4.011	1.326	9 Ainslie's Ref 3
Wind Tuneel Porous Disc						0.903			0.26		2	1.132	10 Sforza
						0.909			0.26		5	1.230	10 Sforza
						0.919			0.26		7.5	1.324	10 Sforza
						0.939			0.26		10	1.341	10 Sforza
						0.400			0.92		2	1.451	10 Sforza
						0.672			0.92		5	1.789	10 Sforza
						0.784			0.92		7.5	1.945	10 Sforza
						0.816			0.92		10	2.021	10 Sforza
						0.835			0.92		12.5	2.107	10 Sforza
						0.876			0.92		15	2.193	10 Sforza

**Table 2: C<sub>T</sub> Correlated Database (yellow highlight implies calculated from Ref'd. data)**

$P_2/P_1$	$u_w$	$C_T$	L	x/Dp
	0.903	0.260		2
	0.909	0.260		5
	0.919	0.260		7.5
	0.939	0.260		10
	<b>C<sub>T</sub> Avg=</b>	<b>0.260</b>		
0.775	0.876	0.340	7	6
0.344	0.657	0.451	2.4	1.4
0.717	0.840	0.451	7	6
0.876	0.923	0.451	7	6
0.876	0.923	0.451	9.4	8.4
0.835	0.903	0.451	9.4	8.4
	<b>C<sub>T</sub> Avg=</b>	<b>0.451</b>		
	0.625	0.540		1.983
	0.737	0.540		3.002
	0.796	0.540		4.098
	0.902	0.540		7.057
	0.640	0.550		3.8
	<b>C<sub>T</sub> Avg=</b>	<b>0.542</b>		
	0.698	0.640		2.971
	0.707	0.600		3.979
	0.834	0.640		4.987
	0.909	0.640		6.768
0.610	0.835	0.615	7	6
0.716	0.888	0.643	7	6
0.500	0.789	0.643	7	6
0.663	0.864	0.643	9.4	8.4
0.162	0.708	0.662	2.4	1.4
0.181	0.570	0.667	2.4	1.4
	0.540	0.670		2.5
	0.548	0.670		2.520
	0.744	0.670		4.011
	0.470	0.670		4.1
	0.701	0.670		6
	0.641	0.650		6.2
	0.870	0.670		6.5
0.645	0.870	0.662	7	6
0.624	0.847	0.667	7	6
0.607	0.840	0.667	7	6
	0.758	0.670		7.5
0.730	0.890	0.667	9.4	8.4
	<b>C<sub>T</sub> Avg=</b>	<b>0.654</b>		
	0.659	0.700		2.971
	0.730	0.700		3.4
	0.770	0.700		4.987
	0.780	0.700		5
	0.903	0.700		6.987
0.505	0.799	0.695	7	6
0.710	0.894	0.695	7	6
0.618	0.853	0.695	7	6
0.634	0.860	0.695	7	6
0.804	0.927	0.695	9.4	8.4
0.735	0.901	0.695	9.4	8.4
0.767	0.913	0.695	9.4	8.4
	0.479	0.714		1
0.539	0.819	0.714	7	6
0.585	0.843	0.714	7	6
0.677	0.882	0.714	7	6
0.700	0.893	0.714	9.4	8.4
0.709	0.894	0.714	9.4	8.4
0.748	0.912	0.714	10.5	9.5
	<b>C<sub>T</sub> Avg=</b>	<b>0.703</b>		
	0.516	0.770		2.5
	0.650	0.760		2.9
	0.504	0.780		2.990
	0.657	0.780		5.043
	0.744	0.770		6
	0.792	0.780		6.799
	0.890	0.760		7.4
	0.882	0.770		7.5
	0.901	0.780		10.167
	0.379	0.820		1

## Appendix A: Horn Rev, MiddleGruden & Vindeby

The data of Table 1 for the three off-shore sites at Horn Rev (80 2MW Vestas 80 wind turbines), Middlegruden (20 2MW Bonus 76 wind turbines) and Vindeby (11 450kW Bonus 36 wind turbines ) employed herein are provided in various forms in Refs. 1-6. For current purposes, only the data downstream of the first turbine was employed.

For the Horn Rev and Middlegrunden sites, the velocities in the wake aft of the first wind turbine were inferred from the second wind turbine's power output and its related power curve. For the current study, only those where the two turbines were aligned to within 1% to 2% of the wind axis were used. This limits the data to a few values of the second turbine's power at a single distance L. Some of Refs. 1-6 provide the measured power output of the second turbine (and others) while some provided the inferred effective wind speed for that power output. In an attempt to account for the upstream influence/disturbance induced by the second wind turbine on its approaching velocity field, in the current analysis, these inferred effective wind speeds were assumed to be representative of the velocity one diameter ahead of the second site turbine, i.e. its distance downstream from the first turbine was reduced by one wake diameter. For the Vendebby site, the velocities in the wakes were measured by a Sodar system and adjustments to the wake locations were not necessary. Figure A-1 provides the measured power curves for both the Vestas 80 and Bonus 76 wind turbines. The power curve for the Bonus 36 was taken here as an area adjusted version of the Bonus 76.

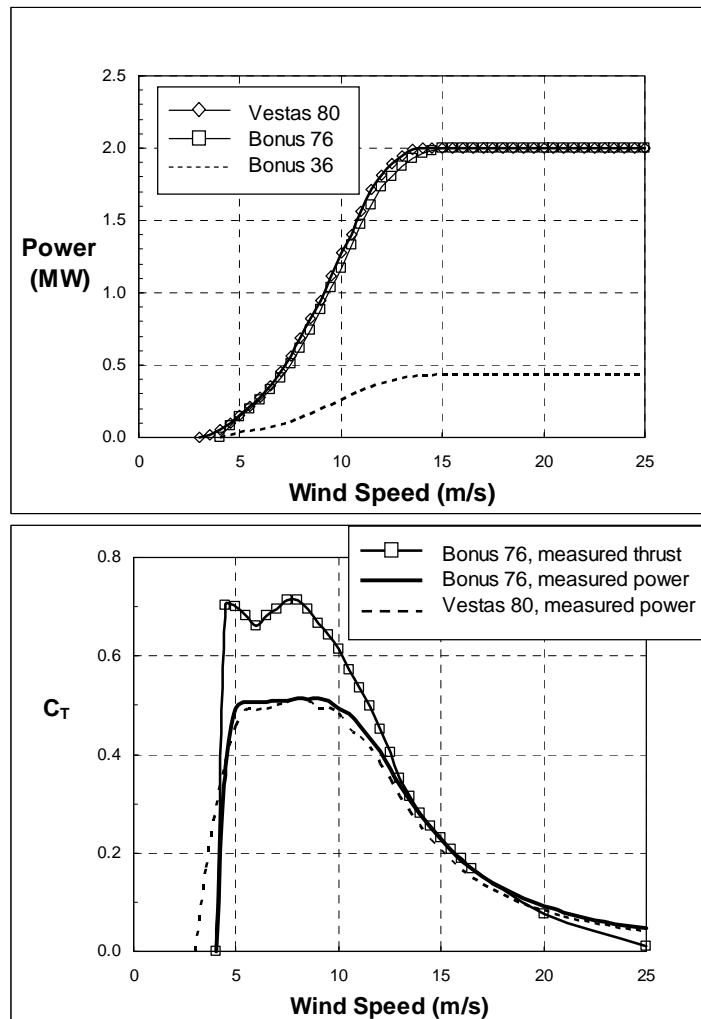


**Fig A-1: Power Curves and Thrust Coefficients**

The Bonus 76 measured thrust coefficient, as provided in Ref. 1, is reproduced in Fig A-1. Also shown are the calculated thrust coefficient values obtained from the measured power levels and related power coefficient using the inverse of Eq. (4b) to write that:

$$C_T = \sqrt{\frac{8C_P}{3}} \cos \left[ \frac{1}{3} A \cos \left( -C_P^{1/2} \sqrt{\frac{27}{32}} \right) + 240^\circ \right], \quad (\text{A-1})$$

where:

$$C_P \equiv \frac{P}{\frac{1}{2} \rho A_p V_a^3}, \quad (\text{A-2})$$

$$C_T \equiv \frac{T}{\frac{1}{2} \rho A_p V_a^2}, \quad (\text{A-3})$$

and  $V_a$  is the effective undisturbed wind speed approaching the turbine. Figure A-2 provides the power coefficients and outlet velocity,  $u_o$ , for all three turbines based on the measured data power curves of Fig A-1. The differences in the measured and calculated power coefficients and thrust coefficients occur because of inherent aerodynamic and mechanical inefficiencies in the respective wind turbine systems, which were found to be operating at approximately an 80% level. This is the source of the significant difference in the inferred levels of outlet velocity shown in Fig. A-2.

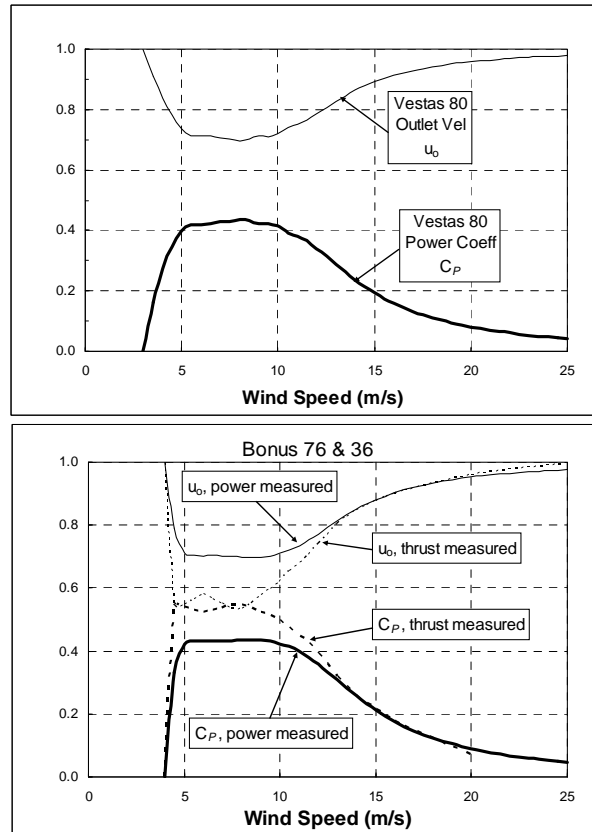


Fig A-2 Vestas and Bonus Performance Parameters

Following Refs. 1-6, the values of the wake widths shown in Table 1 were calculated from momentum and mass conservation along the axial direction assuming a constant pressure state to write that:

$$C_T = \int_0^{\infty} u(1-u) d\left(\frac{D_w}{D_p}\right)^2, \quad (\text{A-4})$$

Which can be integrated to determine an effective wake width by assuming the wake velocity is constant at its centerline value, leading to the relation:

$$\frac{D_w}{D_p} = \sqrt{\frac{C_T}{2u_w(1-u_w)}}, \quad (\text{A-5})$$

## Appendix B: Nibe B and Danwin 180

The data presented in Table 1 for these two wind turbines was reproduced from Refs. 7 & 8, which themselves took the data from reports presented in 1985 and 1996. The results were presented in terms of the velocity profile across the entire wake over a range of measured wind velocities, measured thrust levels and wake distances. For current purposes, only the centerline or nearest-to-centerline velocities were employed for consistency with the other data sets. Additionally, the power curve for the Danwin 180 was provided in Ref. 8 and is reproduced below with all the attendant performance parameters.

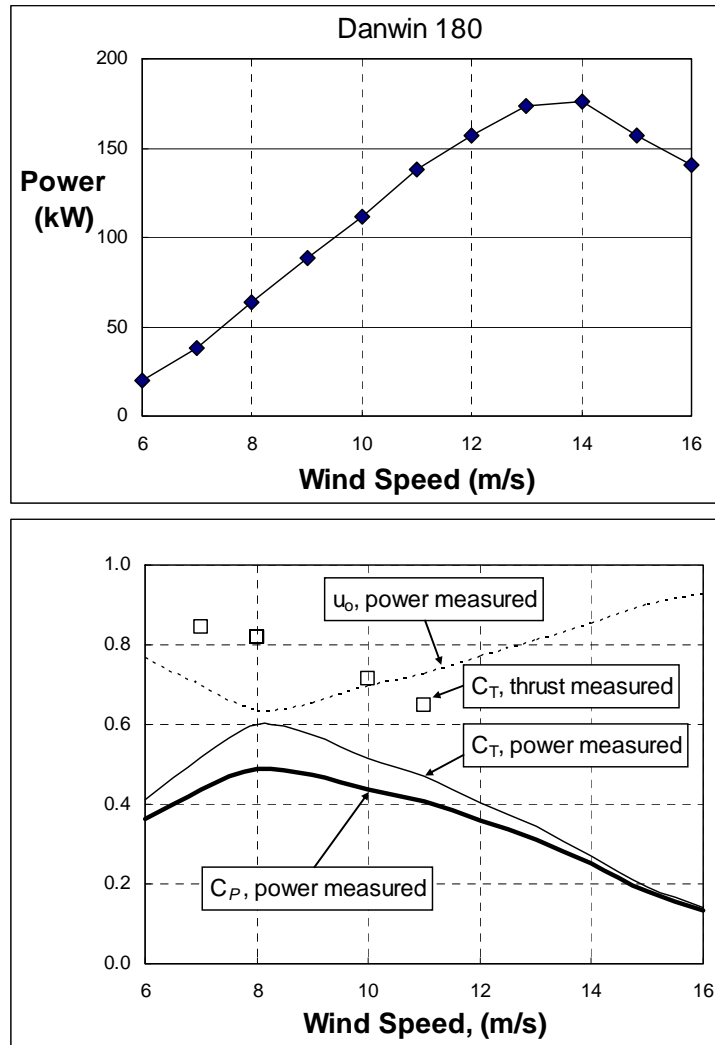


Fig B-1: Danwin 180 Parameters

As in Appendix A, the differences between the measured and calculated thrust coefficients is an indication of the system operating at approximately 80% efficiency. Also, Eq. A-5 was used to calculate the effective wake diameter.

### Appendix C: Ainslie Results

In Ref. 9, Ainslie presents measured wake centerline velocities for a range of configurations from his own organization plus from other organizations and authors, all of which are shown below in Fig. C-1. Ref. 9 presented measured results for rotors in wind tunnels, wind turbine field tests and wind tunnel actuator disc tests. Two cases, however have been excluded from the current set given in Table 1 due to anomalous patterns observed in the data. These are shown in Fig C-1 for the top two cases of the legend on the chart (the very low turbulence level cases) where it is observed in the figure that the measured wake velocities are below the outlet velocities,  $u_o$ , calculated from the stated thrust coefficients. This result is inconsistent with momentum deficit considerations and implies either the reported thrust levels are too low or the velocities reported are in error for these two cases. Ainslie also noted the different behavior for these two cases but indicated that it was possibly due to the low level of turbulence.

Again, the values of the effective wake diameters were calculated using Eq. A-5

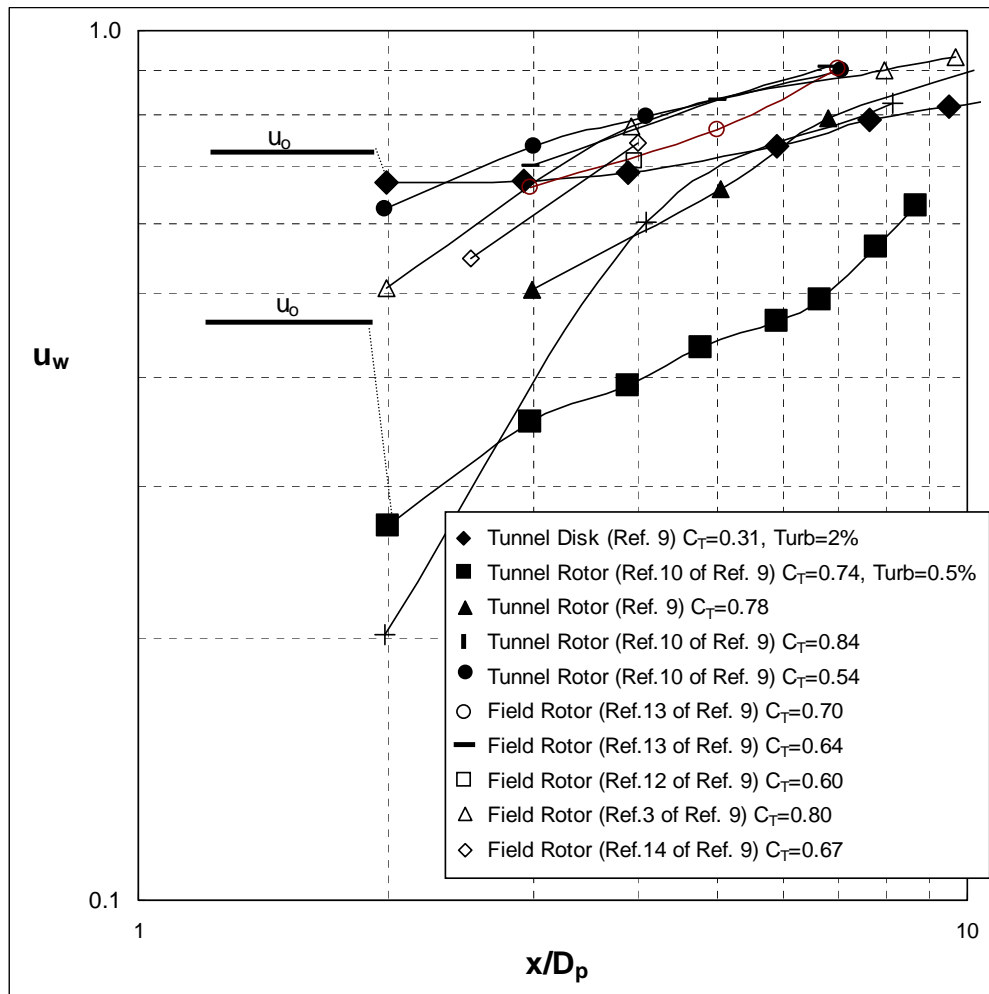


Figure C-1 Data From Ref. 9

### Appendix D: Sforza Porous Disc Wind Tunnel Tests

The data of Ref. 10 presented in Table 1 was acquired in a wind tunnel using a porous disc model to simulate the turbine effect. Because the data was taken in the near the wind tunnel floor to simulate surface boundary layer effects, the wake was found to grow asymmetrically in the vertical and lateral directions. For current purposes, the measured lateral and vertical wake diameter values provided in Ref. 10 were averaged and recorded in Table 1.

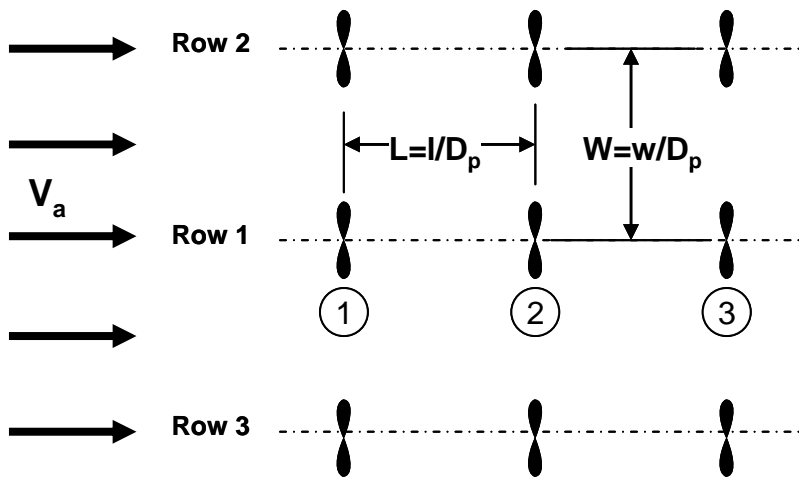


Fig 1. Wind Farm Array

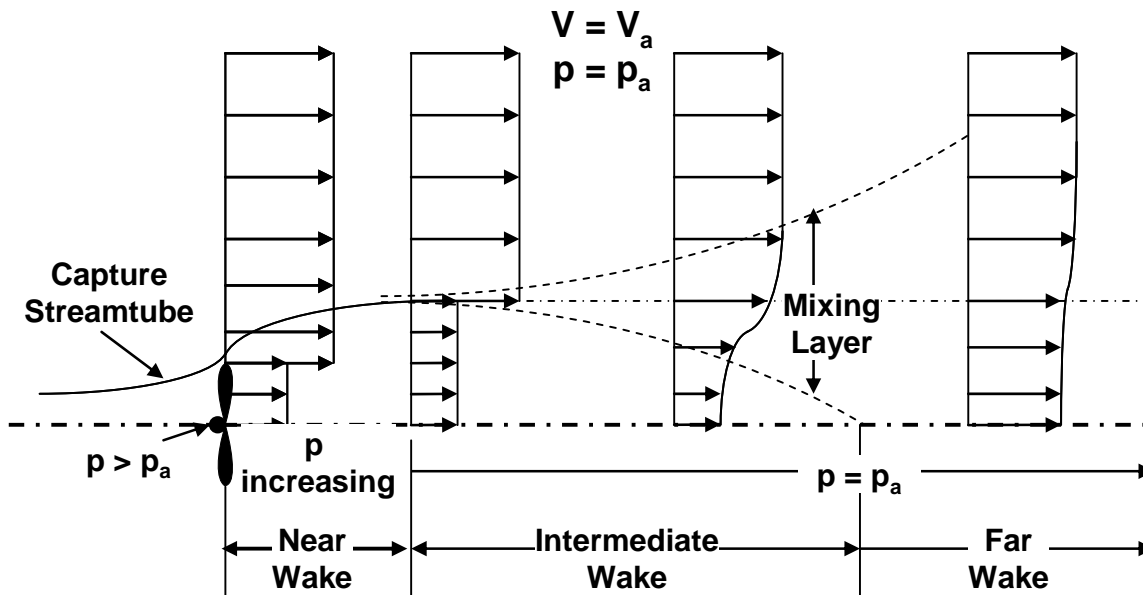
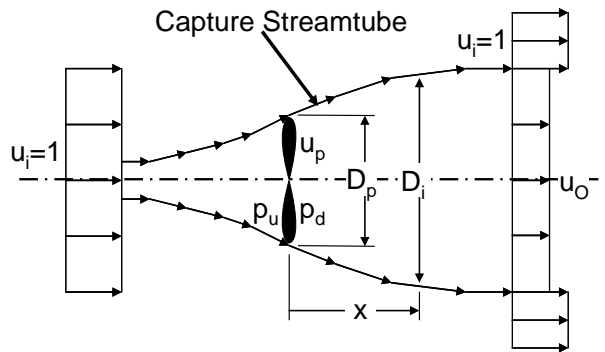
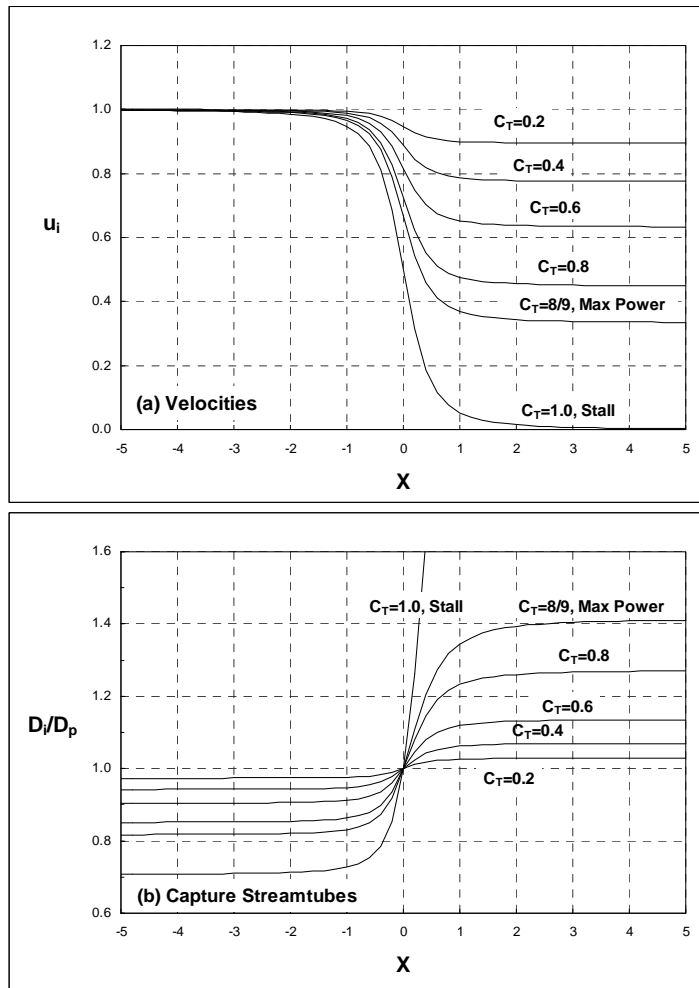


Fig 2. HAWT Wake Flow Structure



**Fig 3. Inviscid Flow Model Nomenclature**



#### 4. Inviscid Model

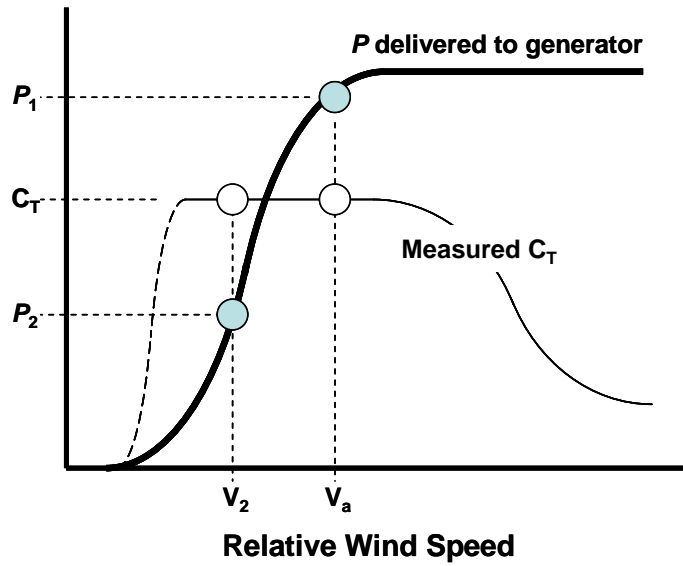


Fig 5. Typical HAWT Power and Thrust Curves

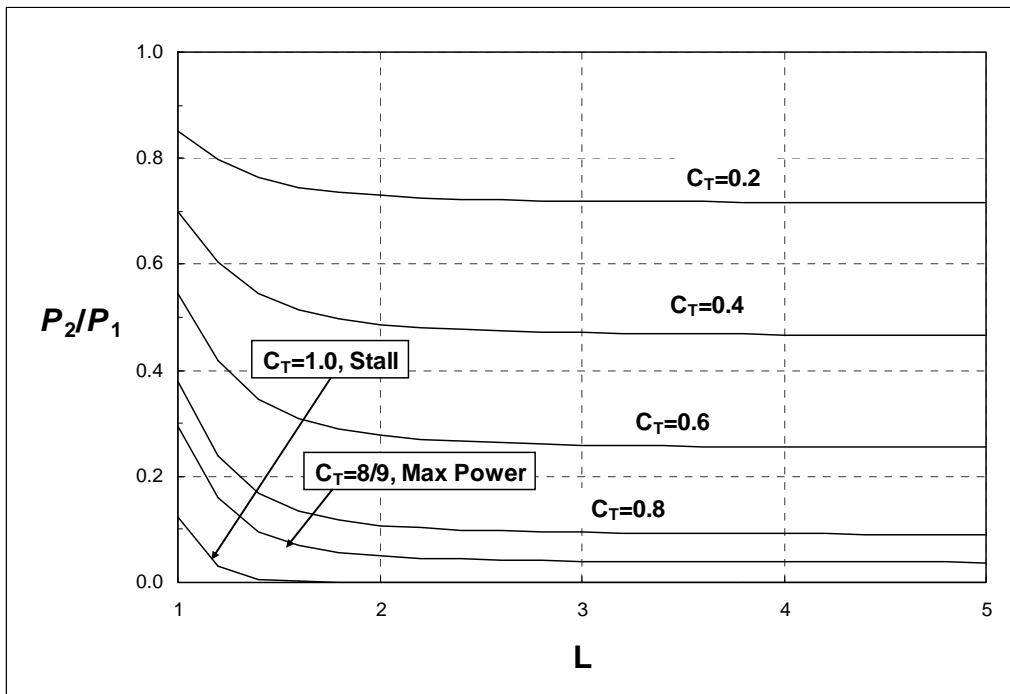


Fig 6. Inviscid Power Ratios

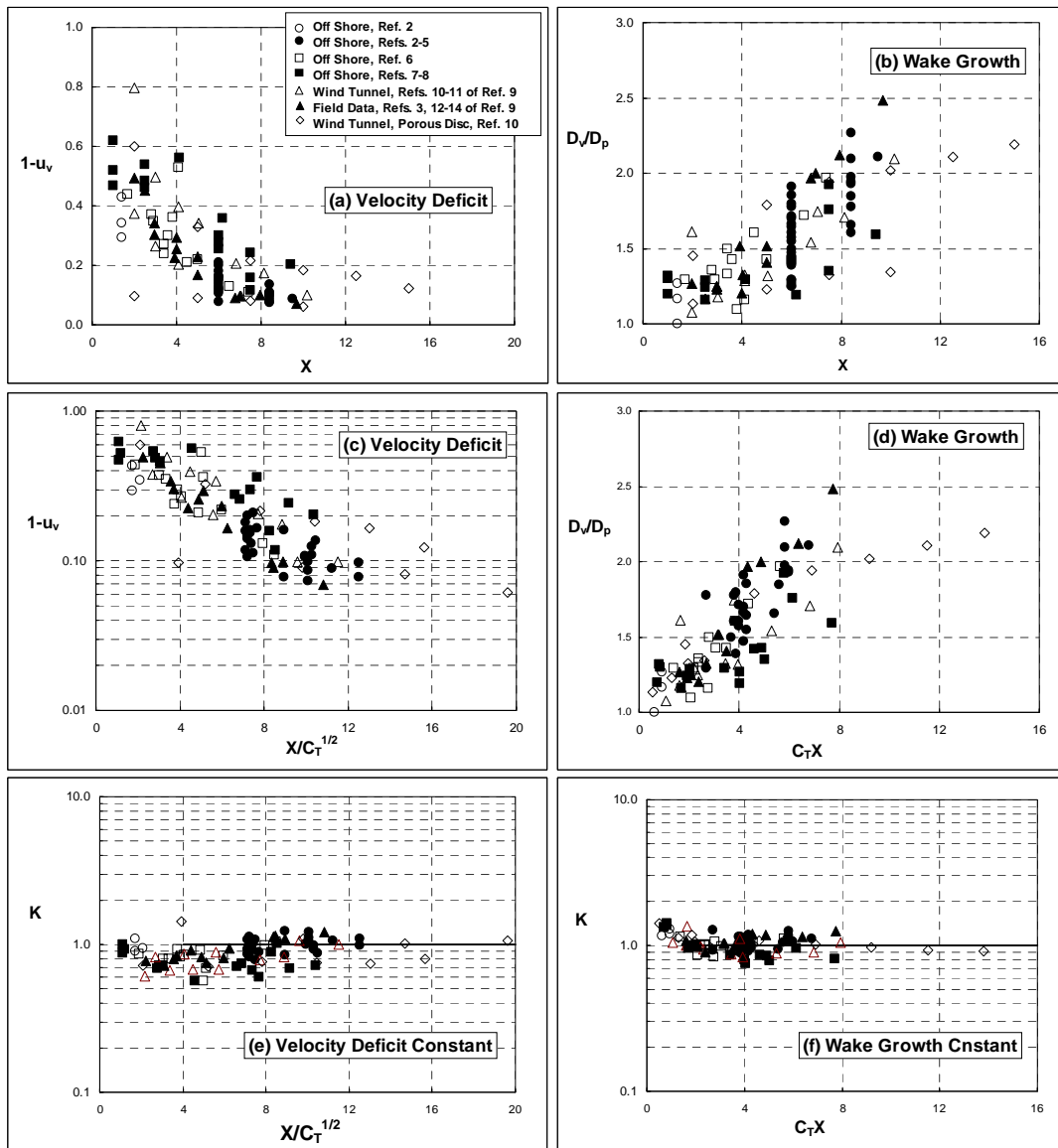


Fig 7. Wake Data

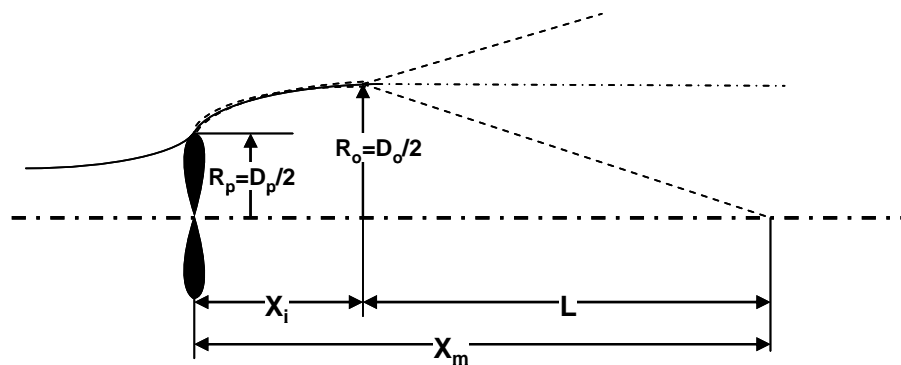


Fig. 8. Intermediate Wake Structure

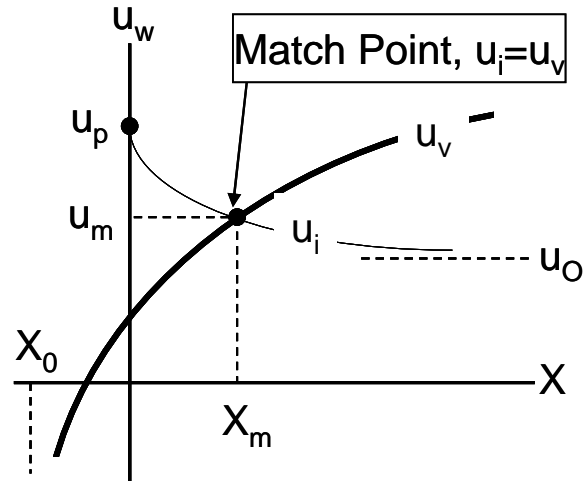


Fig. 9. Composite Wake Solution Structure

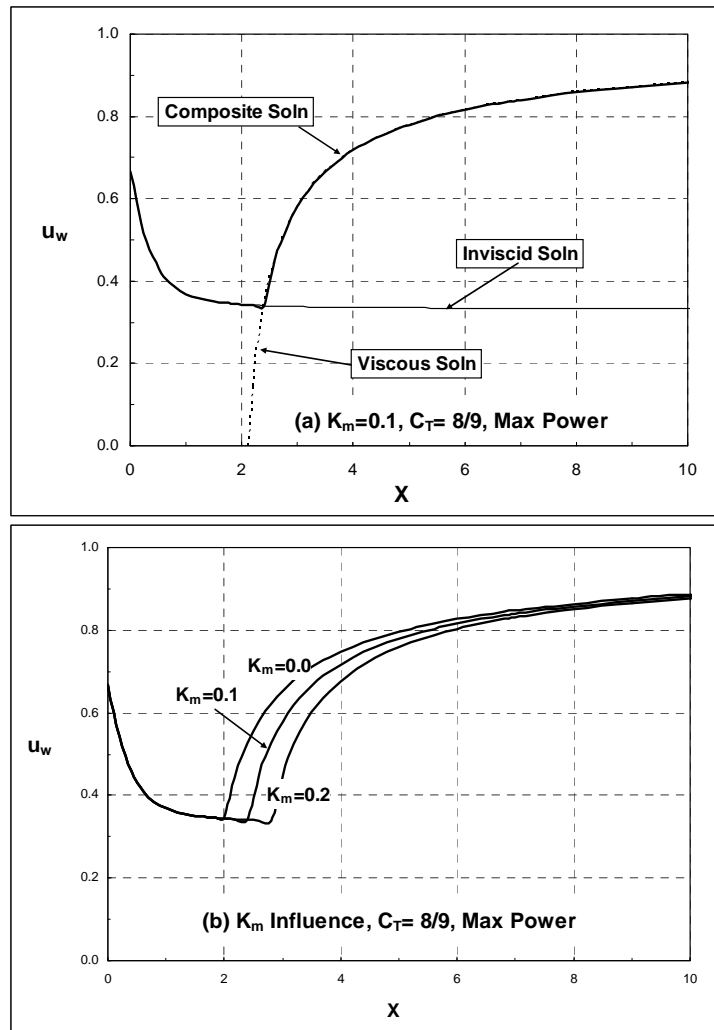


Fig. 10. Model Components and Mixing Length Influence at Max Power

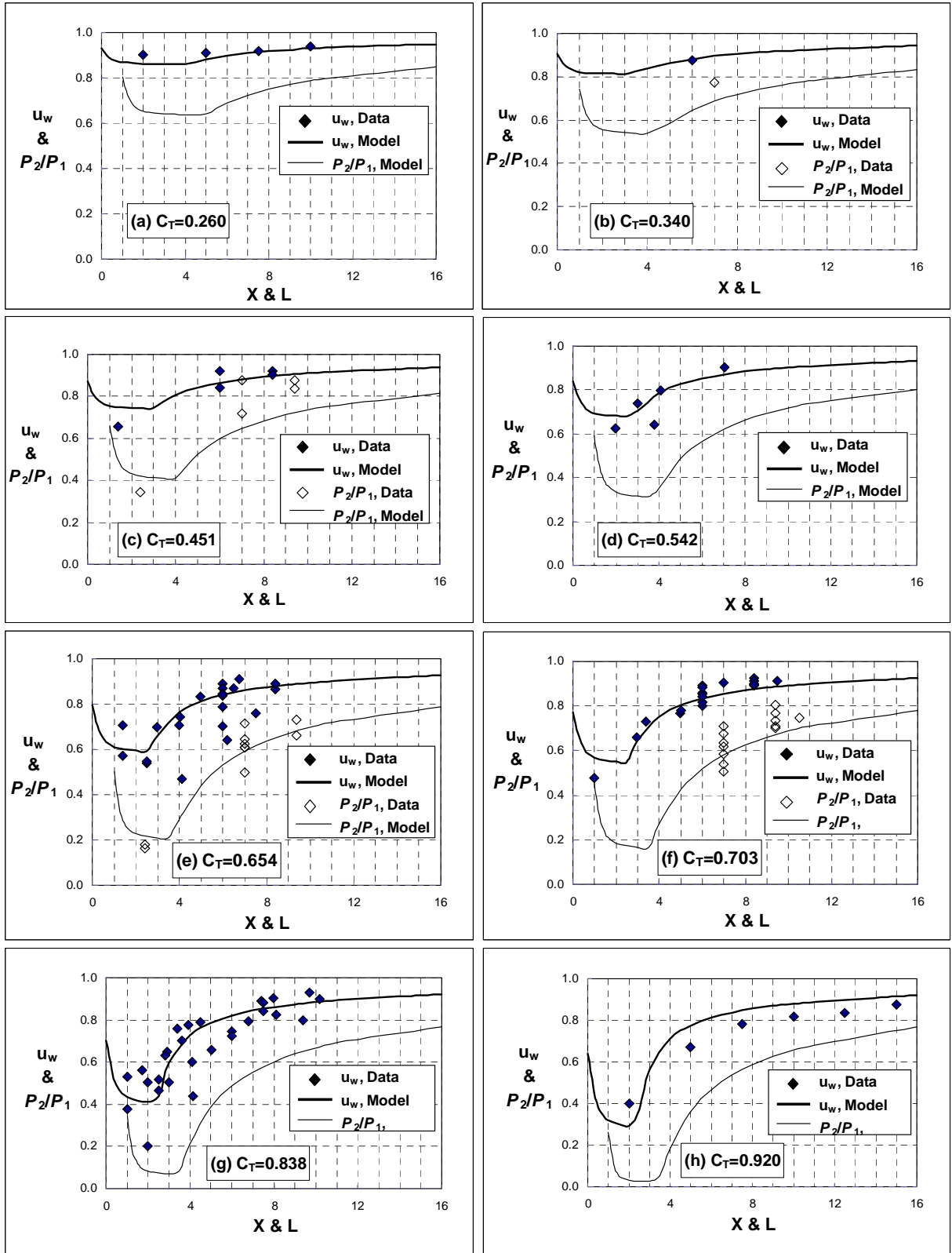
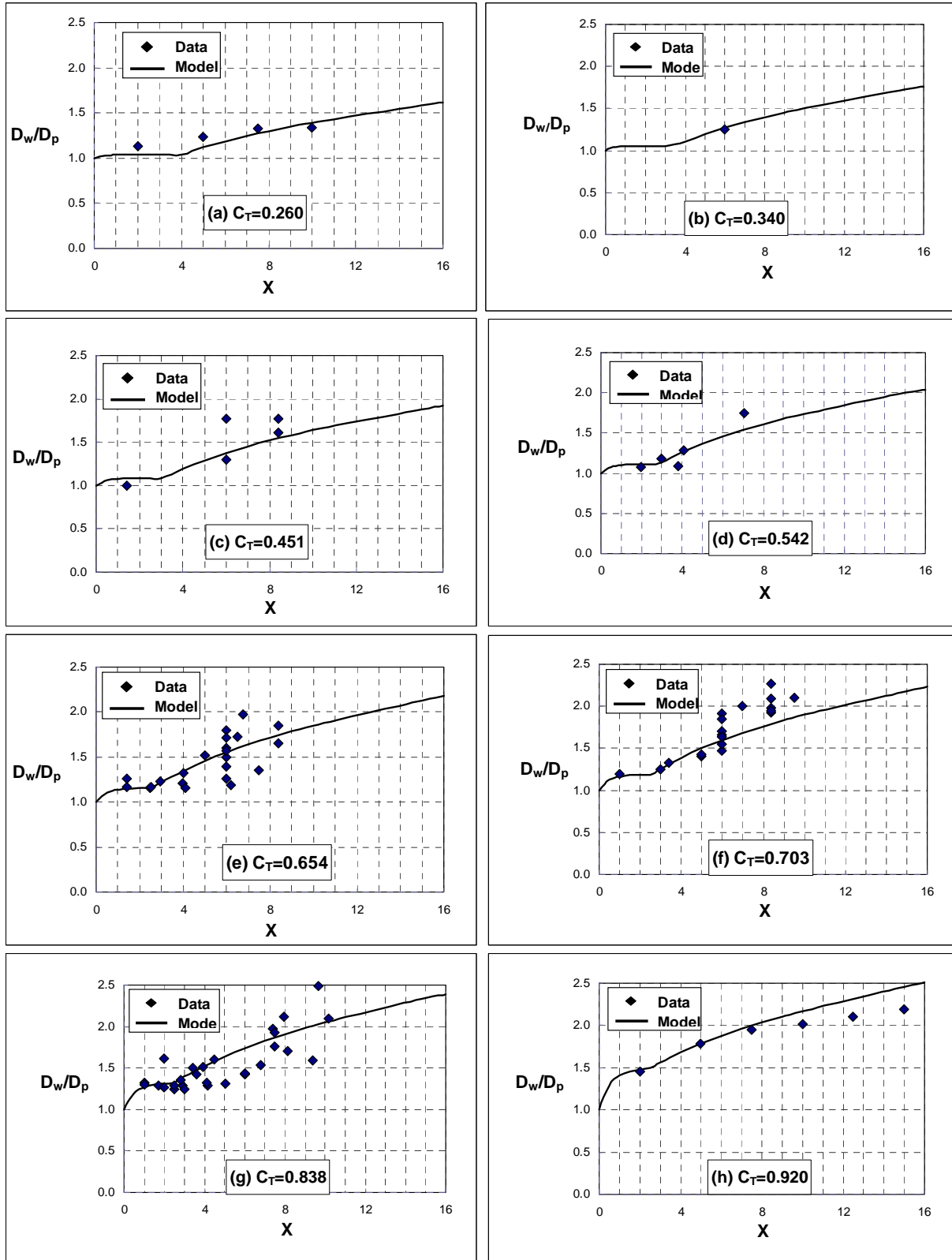


Fig. 11. Velocity & Power Data and Model Comparisons,  $K_m=0.1$ ,  $L_0=1$



**Fig. 12. Wake Growth Data and Model Comparison,  $K_m=0.1$**

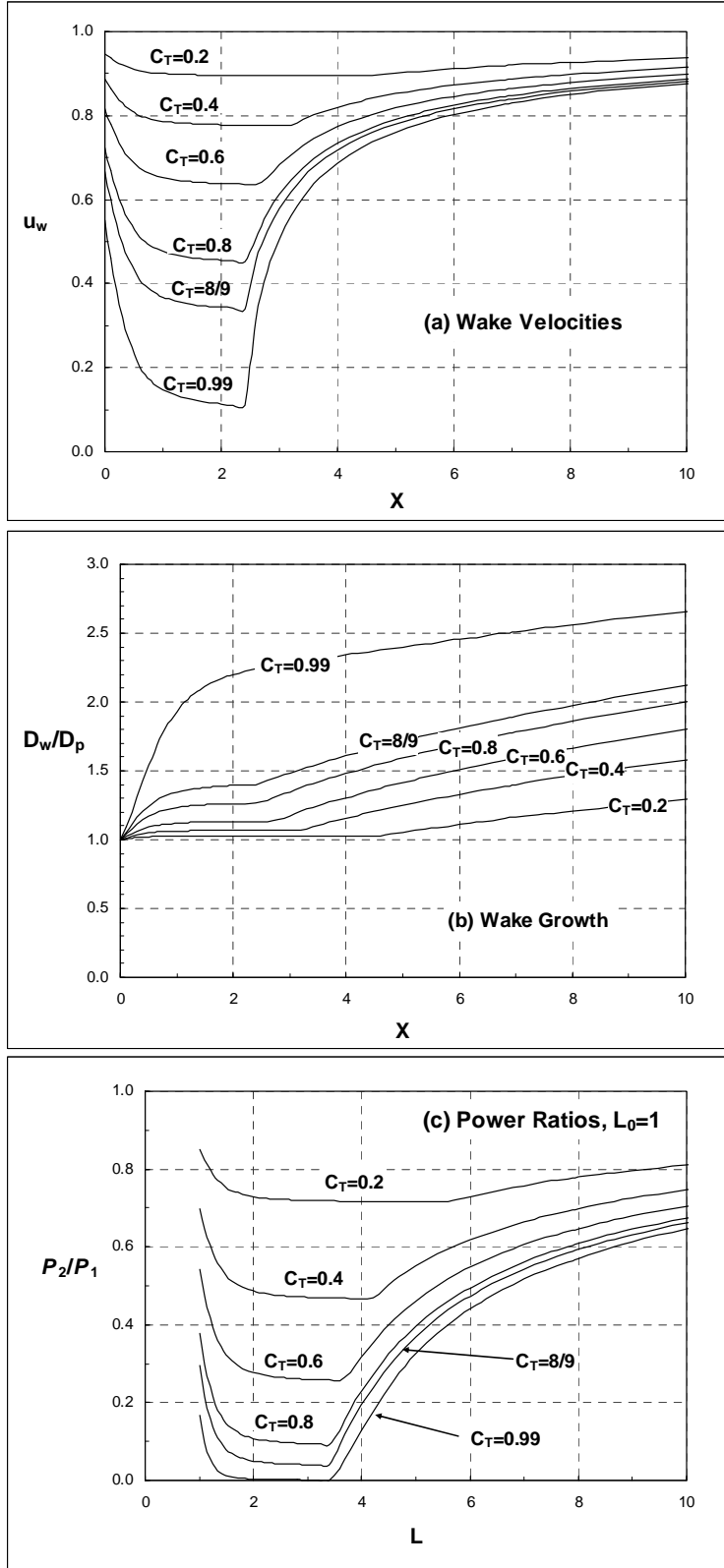


Fig. 13. Model Predictions for  $K_m=0.1$